Frontiers of Physics
https://doi.org/10.1007/s11467-020-0955-7
Front. Phys.
15(3), 33603 (2020)

RESEARCH ARTICLE

Influence of the velocity barrier on the massive Dirac electron transport in a monolayer MoS_2 quantum structure

X.-J. Hao[1], R.-Y. Yuan[1,†], J.-J. Jin[1], Y. Guo[2,3]

[1] *Center for Theoretical Physics, Department of Physics, Capital Normal University, Beijing 100048, China*
[2] *Department of Physics and State Key Laboratory of Low-Dimensional Quantum Physics, Tsinghua University, Beijing 100084, China*
[3] *Collaborative Innovation Center of Quantum Matter, Beijing, China*
Corresponding author. E-mail: [†] *yuanry@cnu.edu.cn*
Received September 25, 2019; accepted February 15, 2020

Using the transfer matrix method, spin- and valley-dependent electron transport properties modulated by the velocity barrier were studied in the normal/ferromagnetic/normal monolayer MoS_2 quantum structure. Based on Snell's Law in optics, we define the velocity barrier as $\xi = v_2/v_1$ by changing the Fermi velocity of the intermediate ferromagnetic region to obtain a deflection condition during the electron transport process in the structure. The results show that both the magnitude and the direction of spin- and valley-dependent electron polarization can be regulated by the velocity barrier. -100% polarization of spin- and valley-dependent electron can be achieved for $\xi > 1$, while 100% polarization can be obtained for $\xi < 1$. Furthermore, it is determined that perfect spin and valley transport always occur at a large incident angle. In addition, the spin- and valley-dependent electron transport considerably depends on the length $k_F L$ and the gate voltage $U(x)$ of the intermediate ferromagnetic region. These findings provide an effective method for designing novel spin and valley electronic devices.

Keywords velocity barrier, monolayer MoS_2, spin, valley, polarization

1 Introduction

In recent years, approaches to efficiently generate and manipulate spin- or valley-polarized are the key issues in spintronics and valleytronics. To solve this problem, various spintronic and valleytronic devices have been designed that are based on two-dimensional materials, and various methods (e.g., optical [1–3], electrical [4–7], magnetic[8–12] and temperature [13] modulation) have been adopted. Among them, the spin- and valley-dependent electron transport properties of monolayer semiconductor transition metal dichalcogenides (TMDCs) MX_2 (M = Mo, W; X = S, Se and Te) have attracted considerable attention [14–18].

Compared to zero band gap graphene, monolayer semiconductor TMDCs have a direct band gap (≈ 1.8 eV) in the visible range. Monolayer MX_2 has reasonable in-plane carrier mobility rate, high thermal stability and good compatibility with standard semiconductor processes [19–22]. At the same time, monolayer semiconductor TMDCs have strong spin-orbit coupling (SOC) [23–28]. For example, this property can produce a strongly valley-dependent spin split ($\lambda = 37.5$ eV) at the top of the valence band along with the reverse asymmetry in monolayer MoS_2. In addition, monolayer semiconductor TMDCs have two intrinsic degrees of freedom for charge and spin [29–31]. Similar to graphene, the first hexagonal Brillouin zone of monolayer MX_2 has a pair of degenerate but not equivalent K and K' valleys at the edge of the conduction band and the valence band. The K and K' valleys are interrelated in the momentum space owing to time-reversal symmetry, which produces good valley degrees of freedom at the edges of electrons and holes. A series of novel phenomena appears based on the valleytronics research, and TMDCs are confirmed to be an ideal energy valleytronics material [32–36].

Owing to these characteristics, TMDCs have broad application prospects in visible light photoluminescence, high-response photodetectors and field effect transistors. For instance, spin- and valley-switching effects can be achieved in the p-doped MoS_2 ferromagnetic/superconducting/ferromagnetic junction [37]. By applying a ferromagnetic field M or an antiferromagnetic field F in the single or double barriers of MoS_2, the transport of ballistic electrons produces different oscillating behaviour [38]. Meanwhile, it has been demonstrated that the spin and valley transport can be manipulated effectively by the gate voltage in a normal/ferromagnetic/normal (N/F/N) monolayer MoS_2 junction [4]. These results provide an

*arXiv: 2003.03718.

© Higher Education Press and Springer-Verlag GmbH Germany, part of Springer Nature 2020

avenue with different parameters for controlling electron transport in MoS_2-based devices.

Similar to the regulation of light, an electric field or a magnetic field, the velocity barrier also has an effective regulation effect on the electron transport properties in a two-dimensional Dirac material; this effect has been studied extensively in graphene-based quantum structures [39–42] and ferromagnetic silicone [43]. Recently, the effect of the velocity barrier on spin and valley polarization transport in monolayer WSe_2 with strong SOC has been investigated, and a new path has been opened for high-efficiency spin and valley polarization in monolayer WSe_2-based electronic devices [44]. However, how the velocity barrier affects the spin- and valley-dependent electron transport properties is still worth exploring.

In this study, using an N/F/N monolayer MoS_2 quantum structure, we investigate the influence of the Fermi velocity barrier on spin- and valley-dependent electron transport. In this case, the velocity barrier can be generated by several methods such as by stretching or extruding the studied material [34], using a superlattice [45, 46] or changing the interaction between surrounding media [47, 48]. The results show that the velocity barrier considerably modulates the transmission and polarization of spin and valley transport, which is more pronounced at large angles.

2 Model and formula

In a given structure, the velocity barrier we consider can be smoothed by corresponding measures; thus, this structure is an ideal and effective model [43]. We assume that the structure width L_y (in the y-direction) is much larger than the ferromagnetic region length L (in the x-direction). Thus, the edge effect of the structure can be neglected, and the fermions have translation invariance in the y-direction. Therefore, the effect under the assumption is only the velocity of movement along the x-direction. We determine the Fermi velocity of each region as follows:

$$v_F(x) = \begin{cases} v_1, & \text{I}, \quad x < 0, \\ v_2, & \text{II}, \quad 0 < x < L, \\ v_1, & \text{III}, \quad x > L, \end{cases} \tag{1}$$

where the Fermi velocity in regions I and III is fixed as $v_1 = 5.3 \times 10^5$ m/s [49–51] and the velocity v_2 in region II is adjustable.

According to Fig. 1(b), it is not difficult to determine that the incident angle and the wave vector of the corresponding region have the relationship of $\tan\theta = k_y/k_{1x}$, and at the same time, the refraction angle also has the relationship of $\varphi = \arctan(k_y/k_{2x})$. To extend Snell's Law in optics to quantum mechanics, a quantum version of Snell's Law is obtained, which provides an interesting research idea for experimentally adjusting the electron transport properties by changing the Fermi velocity in different regions. $\xi = v_2/v_1$ is defined as the ratio of region II to region I and III Fermi velocities. The low-energy effective Hamiltonian of MoS_2 under tight binding approximation can be written as

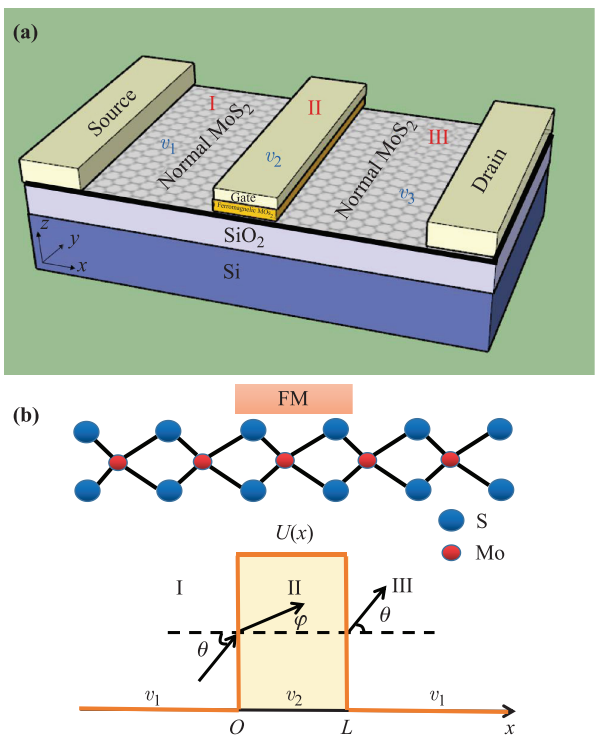


Fig. 1 Schematic diagram of a normal/ferromagnetic/normal (N/F/N) monolayer MoS_2 structure with a velocity barrier. There are a source (left) and a drain (right) in the structure respectively as shown in **(a)**. A gate voltage $U(x)$ is added in the ferromagnetic region to generate electrostatic regulation. The region I and III are normal, L is the length of the intermediate ferromagnetic region. θ and φ are the incident angle and the refraction angle respectively as shown in **(b)**.

$$\begin{aligned} H = {} & \hbar v_F(\tau_z k_x \sigma_x + k_y \sigma_y) + \Delta\sigma_z \\ & + (-\lambda\tau_z s_z \sigma_z + \lambda\tau_z s_z) - s_z h + U, \end{aligned} \tag{2}$$

where $\tau_z = \pm 1$ represents the K and K' valleys respectively, k_x and k_y represent the momentum of the $K(K')$ point, $s_z = \pm 1$ represents the spin up and down, and σ_x, σ_y, σ_z are the Pauli matrix. $\lambda = 37.5$ meV is a spin split induced by SOC at the edge of the valence band, $\Delta = 833$ meV is the band gap caused by the inversion asymmetry between the orbits d_{z^2} and $(d_{x^2-y^2} \pm \mathrm{i}d_{xy})/\sqrt{2}$, and h is the exchange field added in the ferromagnetic region.

Below, we discuss the wave function for different regions. First, according to the setup in Fig. 1, we see that in normal regions, $h = 0$ and $U = 0$. Because the wave function follows translational invariance along the y-direction, we have

$$\psi(x, y) = \begin{pmatrix} \phi_A(x, y) \\ \phi_B(x, y) \end{pmatrix} = \begin{pmatrix} \phi_A(x) \\ \phi_B(x) \end{pmatrix} \mathrm{e}^{\mathrm{i}k_y \cdot y}. \tag{3}$$

Then, by solving the eigenvalue equation $H\psi = E\psi$ with the interface condition, we obtain that the wave function of region I, described as

$$\psi_I = \frac{1}{E_N}\begin{pmatrix}\hbar v_1 k_{1-}\\ E_M\end{pmatrix} \mathrm{e}^{\mathrm{i}k_{1x}\cdot x}\mathrm{e}^{\mathrm{i}k_y\cdot y} + \frac{r}{E_N}\begin{pmatrix}-\hbar v_1 k_{1+}\\ E_M\end{pmatrix} \mathrm{e}^{-\mathrm{i}k_{1x}\cdot x}\mathrm{e}^{\mathrm{i}k_y\cdot y}, \tag{4}$$

where $E_M = E - \Delta$, $E_N^2 = E_M^2 + (\hbar v_1 k_1)^2$, $k_{1+} = \tau_z k_{1x} + \mathrm{i}k_y$, $k_{1-} = \tau_z k_{1x} - \mathrm{i}k_y$.

Similarly, the wave function of region III is described as

$$\psi_{III} = \frac{t}{E_N}\begin{pmatrix}\hbar v_1 k_{1-}\\ E_M\end{pmatrix} \mathrm{e}^{\mathrm{i}k_{1x}\cdot x}\mathrm{e}^{\mathrm{i}k_y\cdot y}. \tag{5}$$

The wave function of region II is described as

$$\psi_{II} = a'\begin{pmatrix}\hbar v_2 k_{2-}\\ E_F\end{pmatrix} \mathrm{e}^{\mathrm{i}k_{2x}\cdot x}\mathrm{e}^{\mathrm{i}k_y\cdot y} + b'\begin{pmatrix}-\hbar v_2 k_{2+}\\ E_F\end{pmatrix} \mathrm{e}^{-\mathrm{i}k_{2x}\cdot x}\mathrm{e}^{\mathrm{i}k_y\cdot y}, \tag{6}$$

where $E_F = E - \Delta - U + s_z h$, $k_{2+} = \tau_z k_{2x} + \mathrm{i}k_y$, $k_{2-} = \tau_z k_{2x} - \mathrm{i}k_y$. Here, we need to emphasize that a', b', r and t are the spin- and the valley-resolved scattering coefficients.

To more conveniently calculate the transmission of the system, we use the transfer matrix method to analyze and express the scattering problem of the given structure. The coordinates on the left and right boundary surfaces of the barrier are $x = 0$ and L respectively. Considering the conservation of local current at the interface of the structure $\boldsymbol{J}(\boldsymbol{r}) = v_F(\boldsymbol{r})\psi(\boldsymbol{r})\boldsymbol{\sigma}\psi(\boldsymbol{r})$, the continuous boundary conditions can be imposed as

$$\sqrt{v_1}\psi_{I(0^-)} = \sqrt{v_2}\psi_{II(0^+)}, \sqrt{v_2}\psi_{II(L^-)} = \sqrt{v_1}\psi_{III(L^+)}. \tag{7}$$

An expression for the transmission probability can be explicitly obtained:

$$T_{\tau_z,s_z}(\theta) = |t|^2 = \left|\frac{2k_2\cos\varphi E_M E_F(k_{1-} + \xi k_{1+})\mathrm{e}^{-\mathrm{i}k_1\cos\theta\cdot L}}{\mathrm{e}^{-\mathrm{i}k_{2x}\cdot L}P + \mathrm{e}^{\mathrm{i}k_{2x}\cdot L}Q}\right|^2, \tag{8}$$

where $P = \xi(E_M E_F k_{1+}k_{2+} + E_M^2 k_2^2) + E_F^2 k_1^2 + E_M E_F k_{1-}k_{2-}$, $Q = \xi(E_M E_F k_{1+}k_{2-} - E_M^2 k_2^2) - E_F^2 k_1^2 + E_M E_F k_{1-}k_{2+}$. $k_1 = \sqrt{(E - \tau_z s_z\lambda)^2 - (\Delta - \tau_z s_z\lambda)^2}/(\hbar v_1)$, $k_2 = \sqrt{(E - \tau_z s_z\lambda + s_z h - U)^2 - (\Delta - \tau_z s_z\lambda)^2}/(\hbar v_2)$.

The spin- and valley-dependent transmissions are defined as

$$T_{\uparrow(\downarrow)} = \frac{T_{K\uparrow(\downarrow)} + T_{K'\uparrow(\downarrow)}}{2}, \tag{9}$$

$$T_{K(K')} = \frac{T_{K(K')\uparrow} + T_{K(K')\downarrow}}{2}. \tag{10}$$

The spin and the valley polarizations are defined as

$$P_S = \frac{T_\uparrow - T_\downarrow}{T_c}, \tag{11}$$

$$P_V = \frac{T_K - T_{K'}}{T_c}, \tag{12}$$

where $T_c = T_{K\uparrow} + T_{K\downarrow} + T_{K'\uparrow} + T_{K'\downarrow}$.

3 Results and discussion

Figure 2 shows spin- and valley-dependent transmissions $T_{\uparrow(\downarrow)}$ and $T_{K(K')}$ as the functions of the incident angle for different velocity barriers. It can be clearly seen that the spin- and valley-dependent transmission in the range of $[-0.5\pi, 0.5\pi]$ is symmetric with the incident angle, namely, $T_{\tau_z,s_z}(\theta) = T_{\tau_z,s_z}(-\theta)$. Therefore, we introduce only the change in electron transmission with ξ in the interval $\theta \in [0, 0.5\pi]$, and it exhibits some interesting phenomena.

In general, with an increase in the velocity barrier ratio ξ shown in Fig. 2, the oscillations of the curves for spin- and valley-dependent electron transmission are both strengthened. This phenomenon indicates that the greater the velocity barrier ratio ξ, the more obvious the resonant effect. This property is confirmed by the transmission expression in Eq. (8). The oscillations, which are not periodic, originate from the unequal factors $\mathrm{e}^{-\mathrm{i}k_{2x}\cdot L}$ and $\mathrm{e}^{\mathrm{i}k_{2x}\cdot L}$ of the transmission coefficient. In addition, the velocity barrier ratio ξ plays an important role in the transmission expression. Therefore, with the appropriate adjustment of the Fermi velocity, the quantum structure has potential applications in resonant tunneling devices.

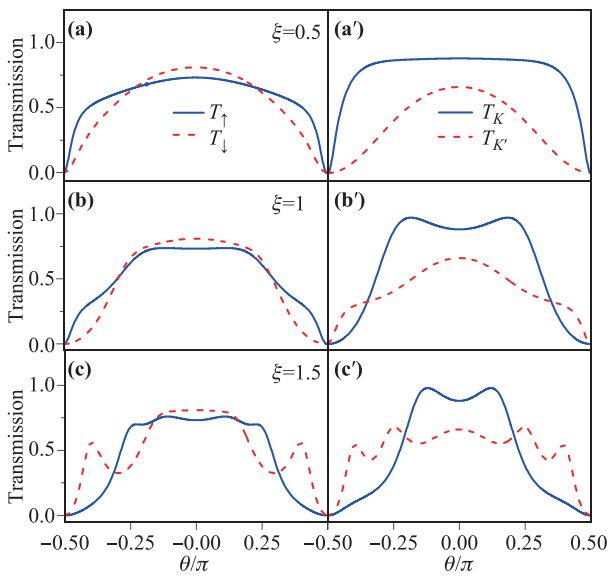


Fig. 2 Spin- and valley-dependent transmission **(a–c)** $T_{\uparrow(\downarrow)}$ and **(a′–c′)** $T_{K(K')}$ as the functions of incident angle θ with different velocity barrier ratio $\xi = 0.5, 1, 1.5$. The other parameters are $L = 7$ nm, $U = -2.0\Delta$, $E = 1.2\Delta$, $h = 0.2\Delta$.

For $\xi = 0.5$ as shown in Figs. 2(a) and (a′), the curves of spin- and valley-dependent electron transmission change smoothly with an increase in the incident angle. The spin-up electron transmission is smaller than the spin-down electron transmission within small incident angles ($\theta < 0.25\pi$), as shown in Fig. 2(a), which indicates that the polarization of spin-down electrons occurs. When the incident angle increases ($\theta > 0.25\pi$), the spin-down electron transmission decreases faster than the spin-up electron transmission, which makes the spin-down electron transmission is smaller than the spin-up electron transmission. It is demonstrated that the reversal effect of spin electron polarization can be achieved at $\theta = 0.25\pi$. However, for $\xi = 0.5$, the valley-dependent transmission versus the incident angle is specific to the spin-dependent transmission. The K valley transmission is always higher than the K' valley transmission in the entire internal $\theta \in [0, 0.5\pi]$ [see Fig. 2(a′)]. Moreover, when the incident angle increases gradually, the K' valley transmission monotonously decreases exponentially. At the same time, the K valley transmission remains nearly 100% for $\theta \in [0, 0.35\pi]$ while decreases rapidly when the incident angle $\theta > 0.35\pi$.

When the velocity barrier ratio $\xi = 1.0$, as shown in Fig. 2(b), the curves of the spin electron transmission have slight oscillations, and the incident angle of polarization inversion is shifted backward ($\theta = 0.30\pi$). Interestingly, for $\xi = 1.0$, the inversion of polarization is also presented in the valley transmission curves. As shown in Fig. 2(b′), with an increase in the incident angle, the K valley transmission is enhanced slightly and then suppressed sharply, and the K' valley transmission decreases monotonously. $T_K > T_{K'}$ within the range of $[0, 0.35\pi]$. When the incident angle $\theta > 0.35\pi$, the K valley transmission decreases faster than the K' valley transmission, which results in $T_K < T_{K'}$, and the polarization of the electron for the K' valley occurs. In addition, we also need to note that 100% transmission for the K valley can be still obtained only when the incident angle $\theta = 0.15\pi$.

With an increase in the Fermi velocity barrier ratio to 1.5, as shown in Figs. 2(c) and (c′), the spin- and valley-dependent electron transmission oscillates clearly. Figure 2(c) shows that spin polarization reversals can be achieved respectively at $\theta = 0.12\pi$ and $\theta = 0.30\pi$. The polarization of the spin-down electron can be obtained in the internal of $[0, 0.12\pi]$ and $[0.30\pi, 0.50\pi]$, while the polarization of the spin-up electron occurs within the range of $[0.12\pi, 0.30\pi]$. However, the curves of the valley electron transmission have only one cross point. The valley polarization inversion is obtained at $\theta = 0.2\pi$, and the angle of the inversion is clearly shifted forward, as shown in Fig. 2(c′). Therefore, these results imply that for the large velocity barrier ratio compared with the valley-dependent electron transmission, the spin-dependent electron transmission is more sensitive to the incident angle. Moreover, it is shown that $T_K \neq 1$ at normal incidence $\theta = 0$, which indicates that perfect transmission does not exist only at normal incidence. Here, we adjust the incident angle to 0.12π, and 100% transmission of the K valley still exists.

To more clearly illustrate how to produce the reversal effect of polarization by modulating the incident angle, we plot the curves of spin- and valley-resolved transmission as the functions of incident angle θ with different velocity barriers, as shown in Fig. 3. According to the transmission expression in Eq. (8), we calculated the values of the incident angle where the reversal effect of polarization appears. For instance, the incident angles $\theta = 0.25\pi$ for $\xi = 0.5$ in Fig. 2(a) and for $\theta = 0.30\pi$ for $\xi = 1$ in Fig. 2(b) are achieved. It is demonstrated that the change of the curves in Fig. 3 is generally the same as the results calculated from the transmission expression. We determine that when the incident angle $\theta < 0.25\pi$, as shown in Fig. 3(a), the transmission of spin electron for the K valley is clearly unchanged. While the incident angle $\theta > 0.25\pi$, the transmission of spin-up electron for the K valley increases slightly to 100%, then decreases rapidly to zero. At the same time, the transmission of spin-down electron for the K valley decreases to zero. $T_{K\uparrow} > T_{K\downarrow}$ in the entire incident angle range. However, for spin electron for the K' valley, all curves of transmission decrease to zero with different amplitudes, as shown in Fig. 3(a′), and $T_{K'\downarrow} > T_{K'\uparrow}$ in the entire range of incident angles. Taking the spin and valley indices in Eqs. (9) and (10) into account, it is determined that at the incident angle of $\theta = 0.25\pi$, the reversal effect of polarization occurs, as shown in Fig. 2(a), for the velocity ratio of $\xi = 0.5$. At other incident angle, the physical origin of the reversal effect of polarization is similar to the one mentioned

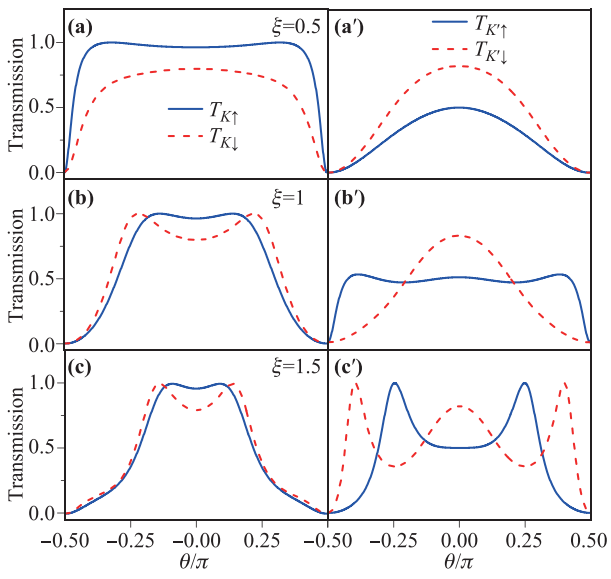


Fig. 3 Spin- and valley-resolved transmission **(a–c)** $T_{K\uparrow(\downarrow)}$ and **(a′–c′)** $T_{K'\uparrow(\downarrow)}$ versus incident angle θ with different velocity barrier ratio $\xi = 0.5, 1, 1.5$. The other parameters are the same as Fig. 2.

above.

To clearly demonstrate the modulation of the velocity barrier ratio ξ on spin- and valley-dependent electron transport, in Fig. 4, we provide the spin and valley polarization P_S(a) and P_V(b) as the functions of the incident angle θ with a different velocity barrier ratio.

For $\xi = 0.5$ and 1.0 with an increase in the incident angle, the spin polarization increases slightly in the positive direction. For $\xi = 1.5$, it is clearly observed that spin polarization increases in the negative direction for $\theta > 0.30\pi$. Furthermore, at the large incident angle, the 100% polarization of spin electron can be achieved for $\xi = 1$, as indicated by the dashed (blue) line, while -100% polarization for spin electron can be obtained [the dotted (green) line] for $\xi = 1.5$ in Fig. 4(a). However, compared to the spin-dependent electron polarization, it is determined that to achieve the 100% polarization for the valley electron, $\xi = 0.5$ is appropriate [the solid (red) line], as shown in Fig. 4(b). Meanwhile, it is determined that -100% valley polarization can be obtained for $\xi = 1.0$, as shown by the dashed (blue) line. These results further demonstrate that the polarization of spin- and valley-dependent electron can be modulated effectively by the velocity barrier.

Figure 4 clearly shows the influence of the velocity barrier on polarization for the spin- and valley-dependent electron can be achieved readily for large incident angles. Thus, we investigate the transport properties of spin- and valley-resolved electron versus length $k_F L$ at the larger incident angle $\theta = 0.48\pi$, as shown in Fig. 5. The left column is the K valley and the right column is the K' valley. First, line-type resonance occurs for spin- and valley-dependent electron transmission. Second, the responses of transmission for spin electron at the K and K' valleys are almost the same for the length $k_F L$ for the corresponding velocity barriers. In addition, it is also shown that the number of line-type resonant peaks tends to decrease with a gradual increase in the velocity barrier ratio ξ. This result indicates that fewer spin- and valley-dependent electron will pass through the barrier.

For the velocity barrier ratio of $\xi = 0.5$ shown in Fig. 5(a), the oscillation frequency versus $k_F L$ and amplitude of the line-type resonance almost overlap, and it is difficult to achieve the spin electron polarization for the K valley. However, spin electron filtering at the K' valley could be achieved at some specific values of $k_F L$, as shown in Fig. 5(a′). For the velocity barrier ratio $\xi = 1$, as shown in Figs. 5(b) and (b′), the spin-down electron of the K and K' valleys pass perfectly through a given device without reflection. This indicates that the spin-down electron transport of the two valleys is independent of the structure length. Moreover, when $k_F L$ is near the values of 3, 7, 11, 15, and 18, the transmission of the spin-up electron in the two valleys suddenly sharply increases to 100%, while at the other values of $k_F L$, $T_{K\uparrow}$ and $T_{K'\uparrow}$ are almost 0. However, when the velocity barrier ratio ξ increases to 1.5, the transmission of spin-down electron in two valleys is suppressed completely. The 100% transmission of spin-up electron for two valleys can be acquired around the values of 5, 10 and 15. Meanwhile, the spin-up electron has a significant change in the number of line-type resonance peaks with an increase in the length $k_F L$.

Therefore, line-type resonance can turn up under the action of the velocity barrier, which is essential for

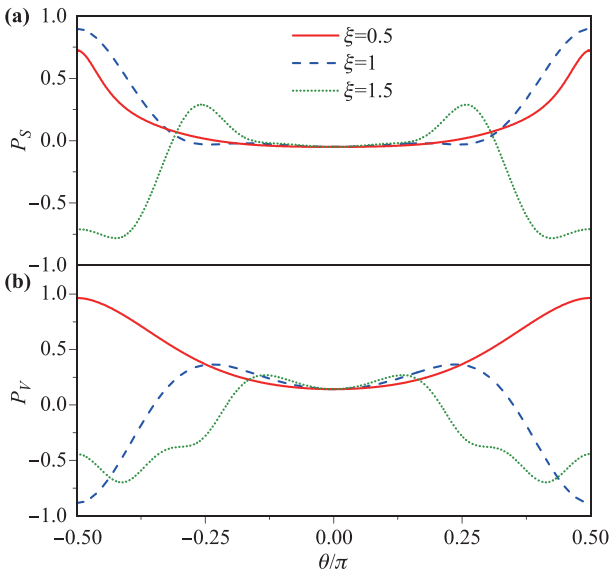


Fig. 4 Spin and valley polarization P_S **(a)** and P_V **(b)** as the functions of incident angle θ with different velocity barrier ratio $\xi = 0.5, 1, 1.5$. The other parameters are the same as Fig. 2.

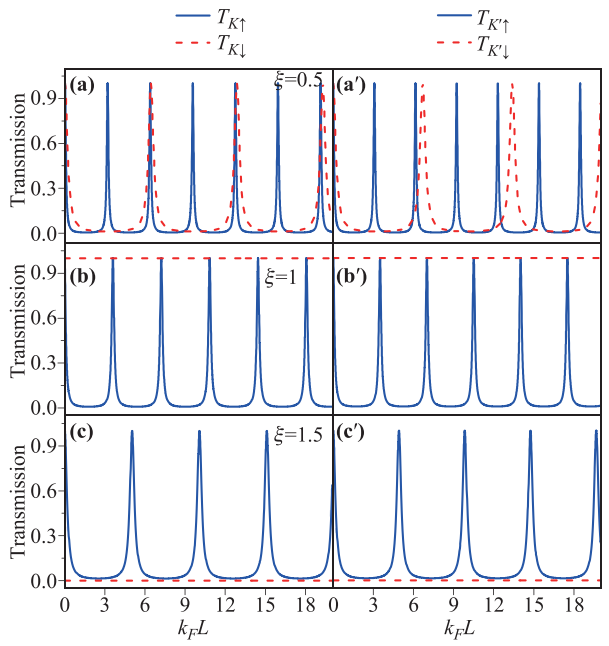


Fig. 5 Spin- and valley-resolved transmission **(a–c)** $T_{K\uparrow(\downarrow)}$ and **(a′–c′)** $T_{K'\uparrow(\downarrow)}$ versus length $k_F L$ with different velocity barrier ratio $\xi = 0.5, 1, 1.5$, where $k_F = E/(\hbar v_F), E = 1.2\Delta$. The other parameters are $\theta = 0.48\pi$, $U = -0.2\Delta$, $h = 0.2\Delta$.

the spin and valley filtering effects at the larger incident angle. This property can be achieved from the line-type resonance conditions $\cos\theta \sim 0$ and $k_2 \cos\varphi \cdot L = n\pi$. Then we can obtain equation $(n\pi\hbar v_F)/L = \sqrt{(E-U-\lambda\tau_z s_z + s_z h)^2 - (E-\lambda\tau_z s_z)^2}$ with the translation invariance in the y-direction. The above-mentioned equation shows that only some massive Dirac electrons equipped with specific energy can tunnel into the interfaces and are strengthened by the line-type resonance at the large incident angle. In addition, based on the transmission expression in Eq. (8), we determined that when the velocity barrier ratio increases, the number of line-type resonant peaks decreases. Otherwise, these interesting phenomena indicate that the spin-down electron can be filtered out within several particular intervals of length $k_F L$ for $\xi = 1$ in the K and K' valleys. Nevertheless, the filtering effect of the spin-up electron can be achieved at the specified length $k_F L$ for $\xi = 1.5$. Consequently, a sensitive current switching device that is based on the spin and valley indices can be theoretically designed in the considered model.

Next, we focus on the the spin- and valley-dependent electron transmissions as the functions of the velocity barrier with various gate voltages. It is illustrated that the transmission of spin and valley electron is not too high with the negative voltage of $U = -2.0\Delta$, as shown in Figs. 6(a) and (a′). $T_{\uparrow(\downarrow)}$ and $T_{K(K')}$ are always below 0.6. For $U = -0.2\Delta$, the electron transmission curves of the two valleys almost overlap. Thus, the effect of the velocity barrier on the electron transmission of the K and K' valleys is almost meaningless, as shown in Fig. 6(b′).

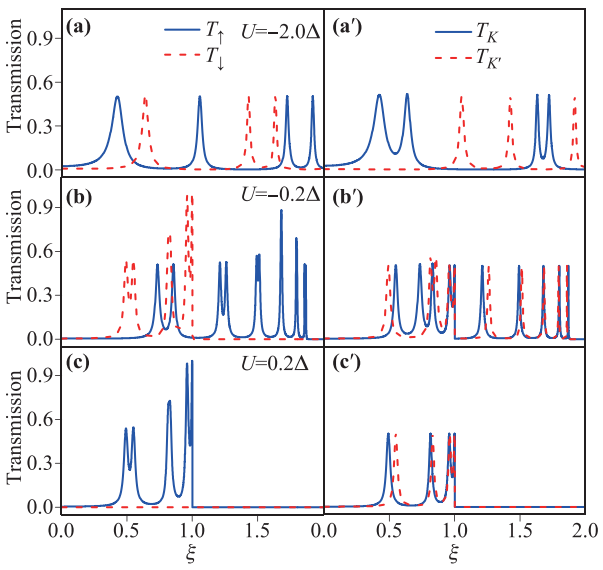


Fig. 6 Spin- and valley-dependent transmission $T_{\uparrow(\downarrow)}$, $T_{K(K')}$ as the functions of velocity barrier ratio ξ with different gate voltage U for $\theta = 0.48\pi$. Here, the parameters are $U = -2.0\Delta$ in (a) and (a′); $U = -0.2\Delta$ in (b) and (b′); $U = 0.2\Delta$ in (c) and (c′). The other parameters are the same as Fig. 2.

However, the spin-dependent electron can achieve perfect filtering for $\xi > 1$ shown in Fig. 6(b). This occurs because the spin-down electron is always suppressed for $\xi > 1$, and the transmission of the spin-up electron is approximately 100% at some special velocity ratios ratios. When the voltage is $U = 0.2\Delta$, the number of line-type resonant peaks is considerably reduced, as shown in Figs. 6(c) and (c′). Of course, it is clear that the positive voltage has a better spin filtering effect on electron because the transmission of spin-down electron in this case is independent of the velocity barrier ratio ξ, and $T_\downarrow$ is always 0 at the given configuration. Thus, for $\xi < 1$, the spin-up current can be obtained by adjusting the corresponding velocity barrier ratio ξ; the transmission of spin-up electron is close to 100% at $\xi = 0.85$ and 1.0. These behaviors have some important practical significance in future spintronic and valleytronic devices.

It is known that conductance is an important and measurable index for the experimental evaluation of spin-valley devices, and it is given as $G_{\tau_z,s_z} = \frac{1}{2}\int_{-\pi/2}^{\pi/2} T_{\tau_z,s_z}\cos\theta \mathrm{d}\theta$ [52]. Therefore, in Fig. 7, we show the results of the spin- and valley-dependent conductance $G_{\uparrow(\downarrow)}$ and $G_{K(K')}$ versus ξ for different gate voltages, where $G_{\uparrow(\downarrow)} = (G_{K\uparrow(\downarrow)} + G_{K'\uparrow(\downarrow)})/2$, $G_{K(K')} = (G_{K(K')\uparrow} + G_{K(K')\downarrow})/2$. It is found that some interesting phenomena also exist in the observable conductance. First, on the whole, with U increasing, the polarizing effect of the conductance for spin-related electron within the range of the considered velocity barrier becomes more and more obvious, while the polarizing effect of the conductance for valley-dependent electron is becoming weaker as shown in Fig. 7. Furthermore, concretely we can see that when the gate voltage $U = -2.0\Delta$, the conductance of spin-dependent electron is sensitive to the modulation of

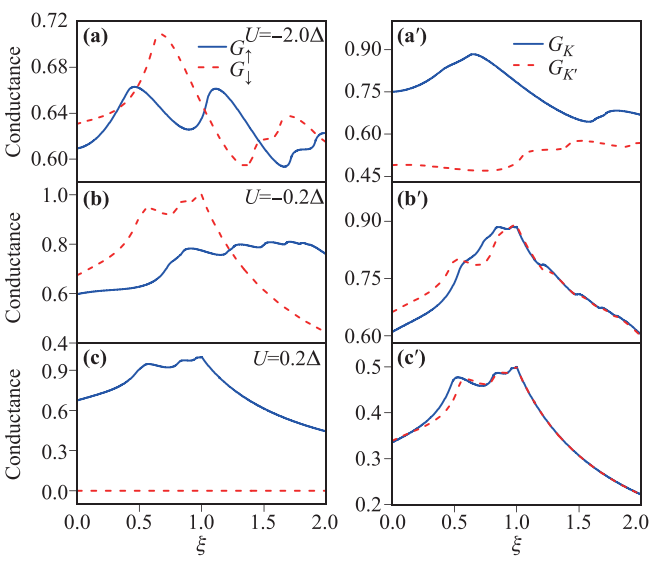


Fig. 7 Spin- and valley-dependent conductance $G_{\uparrow(\downarrow)}$ and $G_{K(K')}$ as the functions of velocity barrier ratio ξ with different gate voltage U. The other parameters are the same as Fig. 2.

Fermi velocity in Fig. 7(a), and there are five points where the situation of polarization inversion occurs. However, the conductance for valley-dependent electron is separated completely in the whole range of ξ seen in the Fig. 7(a′), especially for velocity barrier ratio $\xi = 0.6$. Moreover, we can obtain a positive polarization due to the value of conductance for K valley electron being always higher than that for K' valley electron.

For $U = -0.2\Delta$, there is only one point of polarization inversion for the spin-dependent electron in Fig. 7(b), and the corresponding velocity barrier ratio is 1.2. For $\xi < 1.2$, a negative polarization can be achieved due to $G_\downarrow > G_\uparrow$, while a positive polarization can be obtained for $\xi > 1.2$ because the conductance for spin-down electron sharply declines. In addition, we can find that the polarization for the valley-dependent electron is not good significantly seen in Fig. 7(b′). Particularly, when velocity barrier ratio $\xi > 1.0$, the curves of conductance for two valleys electron are almost overlapped.

When we take the positive voltage $U = 0.2\Delta$, the conductance of spin-down electron has nothing to do with the velocity barrier in Fig. 7(c), and is suppressed completely in the considered range of ξ. Therefore, a perfect filtering effect for spin-up electron can be received. Nevertheless, it is found that the curves of $G_{K(K')}$ are almost the same in the whole range of velocity barrier ratio seen from Fig. 7(c′). Thus, these results provide a practical way for us to manipulate spin and valley currents with different Fermi velocity ratios and voltages in the experiment.

The physical causes of these phenomena may be as follows. Based on the eigenvalue of Eq. (2) $E = U + (\tau_z s_z \lambda - s_z h) \pm \sqrt{(\Delta - \tau_z s_z \lambda)^2 + (\hbar v_F k_2)^2}$, the enhancement of the gate voltage U moves the K' and K bands upward simultaneously, so that the Fermi energy is shifted to only cross the spin-up bands of K' and K valley, this results in that for $U = 0.2\Delta$ the conductance of spin-down electron is zero, only spin-up electron transports, the perfectly full spin-up polarization can be obtained. Meanwhile it leads to a decline of the valley polarization. The enlargement of velocity barrier makes the Fermi energy move relatively to the band edge of spin-down electron at the K' and K valley. Therefore, applying the modulation of Fermi velocity, for $U = -2.0\Delta$, the direction of the spin polarization changes complicatedly, while the valley polarization is just positive. For $U = -0.2\Delta$, as the velocity barrier ratio increases, the Fermi energy at the K' valley only crosses the band of spin-up electron. Thus, the spin polarization has been inverted.

4 Conclusion

In this study, by applying velocity modulation, we investigated the spin- and valley-dependent electron transport properties in a normal/ferromagnetic/normal monolayer MoS_2 quantum structure. To obtain the high spin and valley polarization more efficiently, an appropriate velocity barrier ratio ξ should be considered in the structure. The polarization of spin- and valley-dependent electron can achieve reversal from 100% to −100% with a gradual increase in ξ. By analyzing the transmission of spin and valley electron with an increase in the incident angle, we determine that when the incident angle is larger than 0.16π, the spin and valley polarizations tends to increase gradually, and the perfect polarization effect can be achieved at the larger incident angle. In addition, it is shown that the length $k_F L$ and the gate voltage $U(x)$ of the intermediate ferromagnetic region are also important in the spin- and valley-dependent electron transport. These interesting phenomena provide a certain reference value for experimentally obtaining better electron transport effects using this model.

Acknowledgements This work was supported by NSFC under grants No. 11804236, the General Program of Science and Technology Development Project of Beijing Municipal Education Commission of China under grants No. KM201810028005, and Open Research Fund Program of the State Key Laboratory of Low Dimensional Quantum Physics under grants No. KF201806.

References

1. X. J. Qiu, Z. Z. Cao, J. M. Lei, J. Shen, and C. C. Qin, Optical and Electric Control of Charge and Spin-Valley Transport in Ferromagnetic Silicene Junction, *Superlattices Microstruct.* 109, 735 (2017)
2. M. Tahir, Electrical and optical transport properties of single layer WSe_2, *Physica E* 97, 184 (2017)
3. K. F. Mak, K. L. He, J. Shan, and T. F. Heinz, Control of valley polarization in monolayer MoS_2 by optical helicity, *Nat. Nanotechnol.* 7(8), 494 (2012)
4. H. Li, J. Shao, D. Yao, and G. Yang, Gate-voltage-controlled spin and valley polarization transport in a normal/ferromagnetic/normal MoS_2 junction, *ACS Appl. Mater. Interfaces* 6(3), 1759 (2014)
5. L. F. Sun and Y. Guo, Line-type resonance peaks and their suppression through graphene-based symmetric and asymmetric double barriers, *J. Appl. Phys.* 109(12), 123719 (2011)
6. H. P. Huang, D. Liu, H. M. Zhang, and X. J. Kong, Electronic transport and shot noise in Thue-Morse sequence graphene superlattice, *J. Appl. Phys.* 113(4), 043702 (2013)
7. P. Ye, R. Y. Yuan, Y. Y. Xia, and X. Zhao, Spin and valley transport in the ferromagnetic MoS_2 junctions subjected by the gate voltage, *J. Phys. Conf. Ser.* 827, 012011 (2017)
8. T. Yokoyama, Controllable valley and spin transport in ferromagnetic silicene junctions, *Phys. Rev. B* 87, 241409(R) (2013)

9. L. Majidi and R. Asgari, Valley- and spin-switch effects in molybdenum disulfide superconducting spin valve, *Phys. Rev. B* 90(16), 165440 (2014)
10. H. Haugen, D. Huertas-Hernando, and A. Brataas, Spin transport in proximity-induced ferromagnetic graphene, *Phys. Rev. B* 77(11), 115406 (2008)
11. P. Stepanov, Y. Barlas, S. Che, K. Myhro, G. Voigt, Z. Pi, K. Watanabe, T. Taniguchi, D. Smirnov, F. Zhang, R. K. Lake, A. H. MacDonald, and C. N. Lau, Quantum parity Hall effect in bernal-stacked trilayer graphene, *Proc. Natl. Acad. Sci. USA* 116(21), 10286 (2019)
12. S. Sun, Y. Yu, J. Dang, K. Peng, X. Xie, F. Song, C. Qian, S. Wu, H. Ali, J. Tang, J. Yang, S. Xiao, S. Tian, M. Wang, X. Shan, M. A. Rafiq, C. Wang, and X. Xu, Large g factor in bilayer WS_2 flakes, *Appl. Phys. Lett.* 114(11), 113104 (2019)
13. X. Q. Yu, Z. G. Zhu, J. S. You, T. Low, and G. Su, Topological nonlinear anomalous nernst effect in strained transition metal dichalcogenides, *Phys. Rev. B* 99(20), 201410 (2019)
14. E. I. Rashba, Theory of electrical spin injection: tunnel contacts as a solution of the conductivity mismatch problem, *Phys. Rev. B* 62(24), *R*16267 (2000)
15. G. Schmidt, D. Ferrand, L. W. Molenkamp, A. T. Filip, and B. J. van Wees, Fundamental obstacle for electrical spin injection from a ferromagnetic metal into a diffusive semiconductor, *Phys. Rev. B* 62(8), R4790 (2000)
16. N. Tombros, C. Jozsa, M. Popinciuc, H. T. Jonkman, and B. J. van Wees, Electronic spin transport and spin precession in single graphene layers at room temperature, *Nature* 448(7153), 571 (2007)
17. X. Ma, H. Ai, H. Gao, and X. Zhang, Valley polarization and ferroelectricity in two-dimensional $GaAsC_6$ monolayer, *Phys. Chem. Chem. Phys.* 21, 3954 (2019)
18. K. S. Novoselov, D. V. Andreeva, W. Ren, and G. Shan, Graphene and Other Two-Dimensional Materials, *Front. Phys.* 14, 13301 (2019)
19. A. Splendiani, L. Sun, Y. Zhang, T. Li, J. Kim, C.Y. Chim, G. Galli, and F. Wang, Emerging photoluminescence in monolayer MoS_2, *Nano Lett.* 10(4), 1271 (2010)
20. K. F. Mak, C. Lee, J. Hone, J. Shan, and T. F. Heinz, Atomically thin MoS_2: A new direct-gap semiconductor, *Phys. Rev. Lett.* 105(13), 136805 (2010)
21. G. D. Scholes and G. Rumbles, Excitons in nanoscale systems, *Nat. Mater.* 5(9), 683 (2006)
22. M. Law, J. Goldberger, and P. Yang, Semiconductor nanowires and nanotubes, *Annu. Rev. Mater. Res.* 34(1), 83 (2004)
23. Y. L. Li, J. Ludwig, T. Low, A. Chernikov, X. Cui, G. Arefe, Y. D. Kim, A. M. van der Zande, A. Rigosi, H. M. Hill, S. H. Kim, J. Hone, Z. Li, D. Smirnov, and T. F. Heinz, Valley splitting and polarization by the Zeeman effect in monolayer $MoSe_2$, *Phys. Rev. Lett.* 113(26), 266804 (2014)
24. D. MacNeil, C. Heikes, K. F. Mak, Z. Anderson, A. Kormanyos, V. Zolymi, J. Park, and D. C. Ralph, Breaking of valley degeneracy by magnetic field in monolayer $MoSe_2$, *Phys. Rev. Lett.* 114, 037401 (2015)
25. G. Aivazian, Z. Gong, A. M. Jones, R. L. Chu, J. Yan, D. G. Mandrus, C. W. Zhang, D. Cobden, W. Yao, and X. Xu, Magnetic control of valley pseudospin in monolayer WSe_2, *Nat. Phys.* 11, 141 (2015)
26. A. Srivastava, M. Sidler, A. V. Allain, D. S. Lembke, A. Kis, and A. Imamoğlu, Valley Zeeman effect in elementary optical excitations of monolayer WSe_2, *Nat. Phys.* 11(2), 141 (2015)
27. J. S. Qi, X. Li, Q. Niu, and J. Feng, Giant and tunable valley degeneracy splitting in $MoTe_2$, *Phys. Rev. B* 92(12), 121403 (2015)
28. Z. F. Liu, W. X. Feng, H. L. Xin, Y. L. Gao, P. F. Liu, Y. G. Yao, H. M. Weng, and J. J. Zhao, Two-dimensional spin–valley-coupled Dirac semimetals in functionalized SbAs monolayers, *Mater. Horiz.* 6(4), 781 (2019)
29. F. V. Tikhonenko, D. W. Horsell, R. V. Gorbachev, and A. K. Savchenko, Weak localization in graphene flakes, *Phys. Rev. Lett.* 100(5), 056802 (2008)
30. M. N. Baibich, J. M. Broto, A. Fert, F. N. Van Dau, F. Petroff, P. Etienne, G. Creuzet, A. Friederich, and J. Chazelas, Giant magnetoresistance of (001)Fe/(001)Cr magnetic superlattices, *Phys. Rev. Lett.* 61(21), 2472 (1988)
31. S. Datta and B. Das, Electronic analog of the electron-optic modulator, *Appl. Phys. Lett.* 56(7), 665 (1990)
32. A. Rycerz, J. Tworzydło, and C. W. J. Beenakker, Valley filter and valley valve in graphene, *Nat. Phys.* 3(3), 172 (2007)
33. X. D. Xu, W. Yao, D. Xiao, and T. F. Heinz, Spin and pseudospins in transition metal dichalcogenides, *Nat. Phys.* 10, 343 (2014)
34. A. H. Castro Neto, F. Guinea, N. M. R. Peres, K. S. Novoselov, and A. K. Geim, The electronic properties of graphene, *Rev. Mod. Phys.* 81(1), 109 (2009)
35. H. M. Dong, S. D. Guo, Y. F. Duan, F. Huang, W. Xu, and J. Zhang, Electronic and optical properties of single-layer MoS_2, *Front. Phys.* 13(4), 137307 (2018)
36. G. Y. Wu, N. Y. Lue, and Y. C. Chen, Quantum manipulation of valleys in bilayer graphene, *Phys. Rev. B* 88(12), 125422 (2013)
37. L. Majidi and R. Asgari, Valley- and spin-switch effects in molybdenum disulfide superconducting spin valve, *Phys. Rev. B* 90(16), 165440 (2014)
38. P. M. Krstajić, P. Vasilopoulos, and M. Tahir, Spin- and valley-polarized transport through ferromagnetic and antiferromagnetic barriers on monolayer MoS_2, *Physica E* 75, 317 (2016)
39. R. P. Arnaud, Velocity-modulation control of electron-wave propagation in graphene, *Phys. Rev. B* 81, 073407 (2010)
40. A. Concha and Z. Tešanović, Effect of a velocity barrier on the ballistic transport of Dirac fermions, *Phys. Rev. B* 82(3), 033413 (2010)
41. P. M. Krstaji and P. Vasilopoulos, Ballistic transport through graphene nanostructures of velocity and potential barriers, *J. Phys.: Condes. Matter* 23, 135302 (2011)

42. Y. Wang, Y. Liu, and B. Wang, Resonant tunneling and enhanced Goos–Hänchen shift in a graphene double velocity barrier structure, *Physica E* 53, 186 (2013)
43. J. L. Zhang, W. Fu, K.Y. Wang, S.S. Ke, and H.F. Lü, Effect of a velocity barrier on the spin- and valley-dependent transport in ferromagnetic silicene, *Physica B* 525, 16 (2017)
44. X. J. Qiu, Q. Lv, and Z. Z. Cao, Velocity barrier-controlled of spin-valley polarized transport in monolayer WSe_2 Junction, *Superlattices Microstruct.* 449, 117 (2018)
45. C. H. Park, L. Yang, Y. W. Son, M. L. Cohen, and S. G. Louie, Anisotropic behaviours of massless Dirac fermions in graphene under periodic potentials, *Nat. Phys.* 4(3), 213 (2008)
46. M. Gibertini, A. Singha, V. Pellegrini, M. Polini, G. Vignale, A. Pinczuk, L. N. Pfeiffer, and K. W. West, Engineering artificial graphene in a two-dimensional electron gas, *Phys. Rev. B* 79(24), 241406 (2009)
47. A. Bostwick, T. Ohta, T. Seyller, K. Horn, and E. Rotenberg, Quasiparticle dynamics in graphene, *Nat. Phys.* 3(1), 36 (2007)
48. C. Jang, S. Adam, J. H. Chen, E. D. Williams, S. Das Sarma, and M. S. Fuhrer, Tuning the effective fine structure constant in graphene: Opposing effects of dielectric screening on short- and long-range potential scattering, *Phys. Rev. Lett.* 101(14), 146805 (2008)
49. X. Li, F. Zhang, and Q. Niu, Unconventional quantum Hall effect and tunable spin Hall effect in MoS_2 trilayers, *Phys. Rev. Lett.* 110, 066803 (2013)
50. M. Tahir and U. Schwingenschlögl, Tunable thermoelectricity in monolayers of MoS_2 and other group-VI dichalcogenides, *New J. Phys.* 16(11), 115003 (2014)
51. Z. Li and J. P. Carbotte, Longitudinal and spin-valley Hall optical conductivity in single layer MoS_2, *Phys. Rev. B* 86(20), 205425 (2012)
52. M. Büttiker, Four-terminal phase-coherent conductance, *Phys. Rev. Lett.* 57, 1761 (1986)